



Cite this: *Org. Biomol. Chem.*, 2017, **15**, 6441

Received 3rd May 2017,
Accepted 14th July 2017

DOI: 10.1039/c7ob01068k

rsc.li/obc

^{19}F CEST imaging probes for metal ion detection†

Qiaoli Peng,^a Yaping Yuan,^b Huaibin Zhang,^a Shaowei Bo,^a Yu Li,^a Shizhen Chen,^b Zhigang Yang,^a Xin Zhou^b and Zhong-Xing Jiang ^{*a,b,c}

For detecting metal ions with ^{19}F chemical exchange saturation transfer magnetic resonance imaging (^{19}F CEST MRI), a class of novel fluorinated chelators with diverse fluorine contents and chelation properties were conveniently synthesized on gram scales. Among them, a DTPA-derived chelator with high sensitivity and selectivity was identified as a novel ^{19}F CEST imaging probe for simultaneously detecting multiple metal ions.

Introduction

Metal ions are involved in numerous biological events and, therefore, monitoring the presence of certain metal ions and their local concentrations with novel imaging technology is of great importance for accurately understanding these biological events. Among the many imaging technologies, ^{19}F MRI is very attractive because it provides quantitative images without ionizing radiation, tissue depth limit, and background signals.^{2,3} To this end, some fluorinated chelators, such as 5,5'-difluoro-1,2-bis(*o*-aminophenoxy)ethane-*N,N,N',N'*-tetraacetic acid (5F-BAPTA) and 5,5',6,6'-tetrafluoro-1,2-bis(*o*-aminophenoxy)ethane-*N,N,N',N'*-tetraacetic acid (TF-BAPTA), were employed to monitor metal ions with either ^{19}F NMR by G. A. Smith *et al.*^{1c} and F. A. X. Schanne *et al.*,^{1d} or ^{19}F CEST by M. T. McMahon *et al.*⁶ Although ^{19}F CEST MRI can dramatically amplify the signal of metal ion-bound fluorinated chelators, it is still very challenging to detect metal ions of low concentrations with 5F-BAPTA or TF-BAPTA due to their limited ^{19}F MRI sensitivity. Without using high resolution ^{19}F MRI and extending the scan time, only a very weak ^{19}F signal can be generated from the two fluorine atoms in 5F-BAPTA and TF-BAPTA. In addition, it is very tedious to prepare these fluorinated chelators, especially on gram scales.

Therefore, it is of great importance to develop novel easily available ^{19}F CEST imaging probes with high sensitivity and selectivity for monitoring metal ions at low concentrations.

Herein, a class of fluorinated chelators **1–4** with multiple symmetrical fluorines, a single ^{19}F NMR peak, and controllable chelation properties were designed as novel ^{19}F CEST imaging probes (Fig. 1). Multiple symmetrical fluorines, which collectively give a single ^{19}F NMR peak, were employed as a strong ^{19}F NMR/MRI signal emitter to improve the ^{19}F CEST MRI sensitivity. Ethylenediaminetetraacetic acid (EDTA) and diethylenetriaminepentaacetic acid (DTPA) were selected as the backbones for chelators **1–4** due to their low cost, easy availability, and high chelation selectivity to metal ions.⁴ In order to achieve metal ion selectivity in ^{19}F CEST MRI, the number of chelating groups in chelators **1–4** was tuned by the monoamide and diamide derivatization of EDTA and DTPA, respectively. Besides the carboxylic groups in chelators **1–4**, the hydroxyl and amide groups are also available for metal ion chelation.⁵ Because of the strong electron-withdrawing effect of two adjacent trifluoromethyl groups, the hydroxyl groups in chelators **1–4** are actually very acidic which are good chelating groups for metal ion chelation.^{5c,d} Once the hydroxyl and amide groups in chelators **1–4** are chelated with metal ions, the electron environment of the fluorines changes accordingly which induces a ^{19}F NMR response, *e.g.*, chemical shift change

^aHubei Province Engineering and Technology Research Center for Fluorinated Pharmaceuticals and School of Pharmaceutical Sciences, Wuhan University, Wuhan 430071, China. E-mail: zxjiang@whu.edu.cn

^bState Key Laboratory for Magnetic Resonance and Atomic and Molecular Physics, Wuhan Institute of Physics and Mathematics, Chinese Academy of Sciences, Wuhan 430071, China

^cState Key Laboratory for Modification of Chemical Fibers and Polymer Materials, Dong Hua University, Shanghai 201620, China

† Electronic supplementary information (ESI) available: ^{19}F NMR of chelators in the presence of Cu^{2+} , Fe^{3+} , EDTA and DTPA, association constants of chelators with metal ions, copies of $^1\text{H}/^{13}\text{C}$ NMR and MS/HRMS spectra, and HPLC chromatograms. See DOI: 10.1039/c7ob01068k

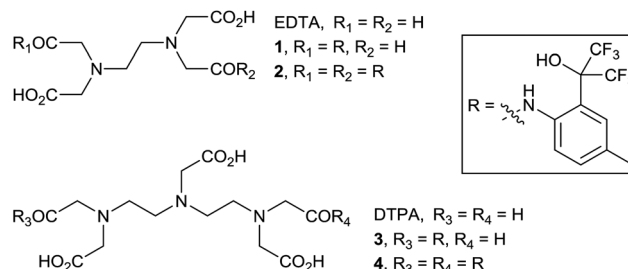


Fig. 1 Structures of fluorinated chelators **1–4**.

($\Delta\omega$) and line broadening. If the exchange rate between the metal ion-bound chelator and free chelator is slow enough ($k_{\text{ex}} < \Delta\omega$), a new peak will show up on the ^{19}F NMR spectra of chelators 1–4. According to the mechanism of ^{19}F ion-CEST MRI,⁶ *i.e.*, using a radiofrequency to saturate the new peak from the metal ion-bound chelators and detecting the saturation transfer to the free chelators, the signal of bound metal ions can be dramatically amplified.

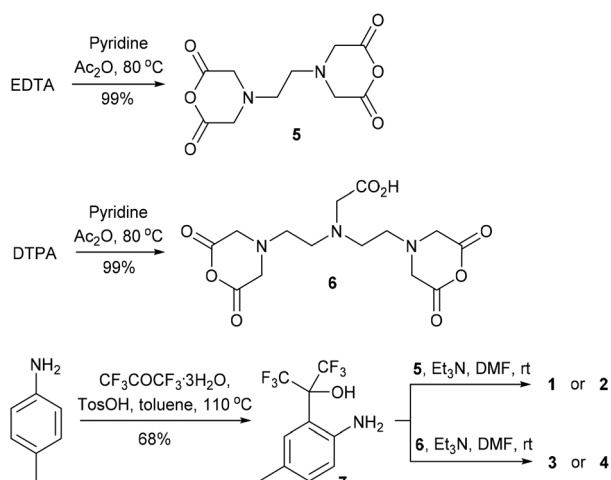
Results and discussion

A convenient and scalable synthesis of fluorinated chelators 1–4 was developed, in which the amidation reaction between dianhydrides 5, 6 and fluorinated aniline 7, respectively, was employed as the key step (Scheme 1). Fresh dianhydrides 5 and 6, which are also commercially available, were prepared by dehydration of EDTA and DTPA with acetic anhydride in the presence of pyridine, respectively.⁷ Fluorinated amine 7 with a bis(trifluoromethyl)-carbinol moiety was then prepared through a Friedel–Crafts reaction of hexafluoroacetone trihydrate on 4-methylaniline in the presence of *p*-toluenesulfonic acid.⁸ Monoazides 1, 3 and diamides 2, 4 were selectively prepared by tuning the relative amount of amine 7 and dianhydrides 5, 6 during the amidation reaction, respectively. It is noteworthy that the hydroxyl group in 7 is very inert during the amidation reactions because the two adjacent trifluoromethyl groups dramatically lowered the reactivity by increasing its acidity and steric hindrance. To guarantee the high purity of the fluorinated chelators 1–4, the amidation reaction mixtures were purified with preparative HPLC. Finally, fluorinated chelators 1–4 were prepared on 0.61–2.25 gram scales with good yields and high purities.

As the poor water solubility of fluorinated compounds always limited their application in biological systems, the water solubility of chelators 1–4 was then investigated. It was found that the water solubility of chelators 1–4 is closely

related to their fluorine contents (F%). Low F% chelators 1 (21%) and 3 (18%) are soluble in water in a wide pH range of 0 to 14, while high F% chelators 2 (28%) and 4 (25%) are soluble in water only at pH above 6 and 5, respectively. Therefore, all the fluorinated chelators 1–4 have no solubility issue for a downstream ^{19}F NMR/MRI study around the physiological pH.

As expected, each chelator produces a single ^{19}F NMR peak from multiple symmetrical fluorines which is ideal for detecting the chelator at low concentrations (red peaks in Fig. 2). To study the chelation effects on ^{19}F NMR, the ^{19}F NMR spectra of chelators 1–4 in the presence of Mg^{2+} , Ca^{2+} , Fe^{3+} , Cu^{2+} , and Zn^{2+} were collected. After chelating with Fe^{3+} and Cu^{2+} , no observable new ^{19}F NMR peaks can be detected on the ^{19}F NMR spectra of chelators 1–4 (Fig. S1 in the ESI†). In contrast, well-defined new ^{19}F NMR peaks on the ^{19}F NMR spectra of chelators 1–4 were detected in the presence of Mg^{2+} , Ca^{2+} and Zn^{2+} (Fig. 2). For chelators 1–3, multiple chelation peaks were detected in the presence of Ca^{2+} and Zn^{2+} which correspond to multiple species formed between the chelator and the metal ion.⁹ It is very important to point out that each of the free chelators 1–4 produces a singlet ^{19}F NMR peak around -74.4 ppm, respectively, with a small $\Delta\omega$ of 0.2 ppm despite their structural difference. Even after chelating with metal ions, the $\Delta\omega$ between free chelators and metal ion bound-chelators is less than 1 ppm. The small $\Delta\omega$ values indicate that metal ion chelation has limited influence on the electron environment of the fluorines because multiple C–C single bonds have significantly blocked the chelation effect. As a comparison, the $\Delta\omega$ of free TF-BAPTA and Zn^{2+} -bound TF-BAPTA reaches 10.5 ppm because the aromatic system can efficiently transfer the chelation effect to fluorines.⁶ The appearance of well-defined new ^{19}F NMR peaks also indicates



Scheme 1 Synthesis of fluorinated chelators 1–4.

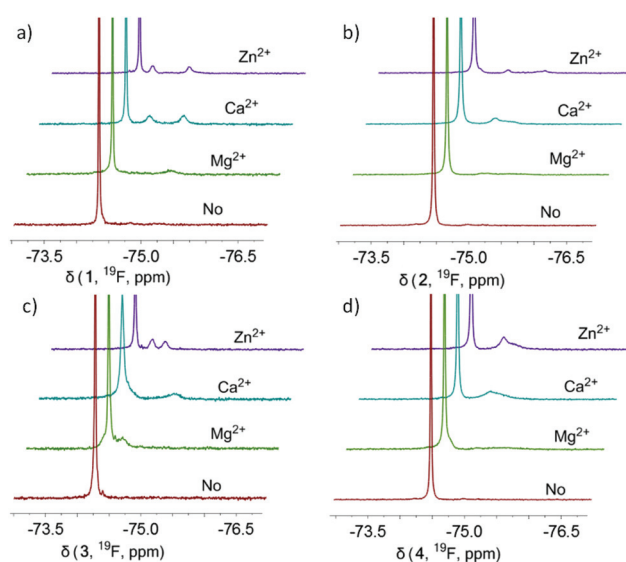


Fig. 2 ^{19}F NMR of free chelators (red peaks) and Mg^{2+} , Ca^{2+} , and Zn^{2+} -bound chelators 1 (a), 2 (b), 3 (c), and 4 (d). Each sample contained 0.8 mM metal ions and 4.0 mM chelators in 40 mM Hepes buffer at pH 7.2.

that the exchange between the metal ion-bound chelators and free chelators is very slow ($k_{ex} < \Delta\omega$), which is fit for generating the ^{19}F CEST contrast. Chelator **4** was chosen for a downstream ^{19}F CEST study for two reasons. On the one hand, chelator **4** has a singlet ^{19}F NMR peak from twelve fluorines which can dramatically improve the ^{19}F MRI sensitivity and lower the detectable concentration. On the other hand, a single ^{19}F NMR peak from the free and metal ion-bound chelator **4**, respectively, can simplify the ^{19}F CEST process by avoiding the suppression of nearby peaks (Fig. 2d).

The influence factors, including metal ion concentration, pH, temperature, and the addition of fast exchange metal ions, on the ^{19}F NMR of free and ion-bound chelator **4** were also studied. The Ca^{2+} concentration-dependent ^{19}F NMR showed that chelator **4** and Ca^{2+} formed a complex with a broad ^{19}F NMR peak around -74.9 ppm. A well-defined peak can be observed when the Ca^{2+} /chelator ratio is larger than 1/10 (Fig. 3a). The pH-dependent ^{19}F NMR showed that pH 6.0–7.5, which is within the physiological pH, is the best range for detecting the Ca^{2+} -bound chelator **4** with ^{19}F NMR (Fig. 3b). It is noteworthy that very little chemical shift change was found in the range of pH 6.0–7.5, *i.e.* $\Delta\omega = 0.07$ for Ca^{2+} -bound and free chelator **4**, respectively. The addition of fast exchange ions K^+ resulted in no observable ^{19}F NMR line broadening or chemical shift change, while the addition of Mg^{2+} resulted in observable ^{19}F NMR line broadening of the free chelator **4** peak (Fig. 3c). The temperature-dependent ^{19}F NMR showed no line broadening for free chelator **4**, while it showed obvious line sharpening for Ca^{2+} chelator **4** at elevated temperature (Fig. 3d).¹⁰ It was also found that in the range of 283 K to 310 K, an obvious chemical shift change ($\Delta\omega = 0.2$ ppm) was observed for both free and Ca^{2+} -bound chelator **4**. In contrast

to 5F-BAPTA of which the ^{19}F NMR chemical shift is very sensitive to pH, temperature, and fast exchange ions, chelator **4** shows little response to these influence factors except for temperature. Therefore, using chelator **4** in ^{19}F NMR and ^{19}F MRI can actually avoid the image artifact and chemical shift calibration, which dramatically simplifies the ^{19}F NMR and ^{19}F CEST MRI process.

To evaluate the ^{19}F metal ion induced CEST (iCEST) effect of metal ions, the pH and metal ion-dependent Z-spectra of chelator **4** were collected. On the one hand, an iCEST effect of Ca^{2+} at $\Delta\omega = 0.4$ ppm was observed from the pH-dependent Z-spectra (Fig. 4a–d). Because Ca^{2+} -bound chelator **4** dissociates under weak acidic conditions, a pronounced iCEST effect can only be found when pH > 6.0. On the other hand, an iCEST effect can be found for other selected metal ions. For Mg^{2+} , a well-defined iCEST effect on chelator **4** at $\Delta\omega = 0.6$ ppm was found (Fig. 4f), while an iCEST effect was found at $\Delta\omega = 0.4$ ppm for Zn^{2+} (Fig. 4h). Thus, by tuning the frequency of a saturation pulse, it is feasible for chelator **4** to selectively detect Mg^{2+} , Ca^{2+} , and Zn^{2+} using ^{19}F CEST MRI.

^{19}F iCEST MRI on metal ions was carried out on a 9.4 T scanner. Firstly, selective ^{19}F iCEST MRI of chelator **4** on Mg^{2+} , Ca^{2+} , and Zn^{2+} was studied (Fig. 5). ^{19}F MRI of four tubes

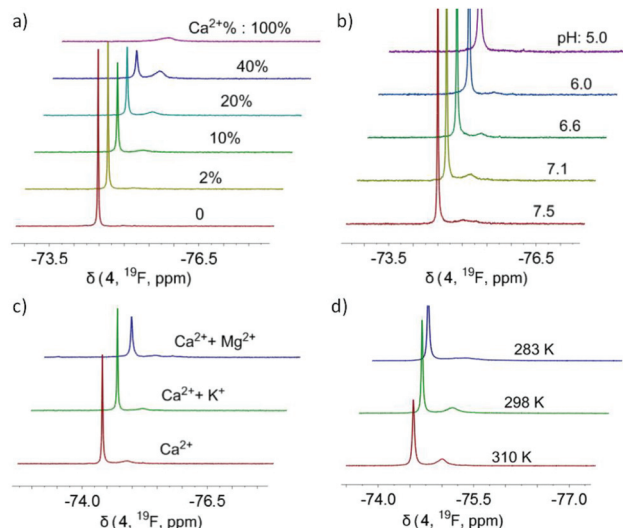


Fig. 3 Concentration (a, $\text{Ca}^{2+}\% = [\text{Ca}^{2+}]/[\text{chelator } \mathbf{4}] \times 100\%$), pH (b), additive (c, 100 mM K^+ and 0.8 mM Mg^{2+}), and temperature-dependent (d) ^{19}F NMR of chelators **4**. Each sample contained 4.0 mM chelators **4** and 0.4 mM Ca^{2+} (b, c) or 0.8 mM Ca^{2+} (d) in 40 mM Hepes buffer at pH 7.2.

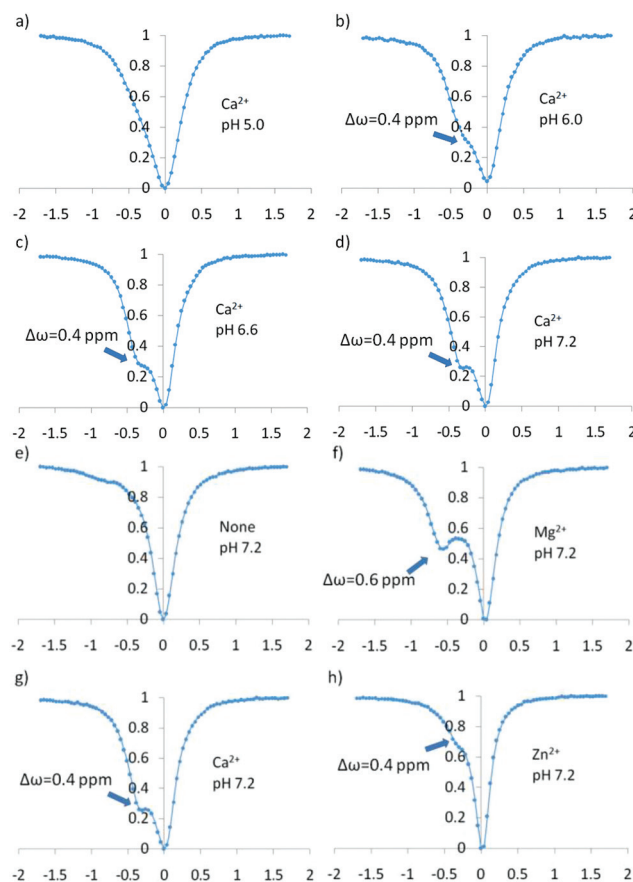


Fig. 4 pH (a–d) and metal ion-dependent (e, none; f, Mg^{2+} ; g, Ca^{2+} ; h, Zn^{2+}) Z-spectra of chelator **4** and M^{2+} . Each sample contained 2.0 mM chelator **4** and 0.2 mM M^{2+} in 40 mM Hepes buffer at the indicated pH.

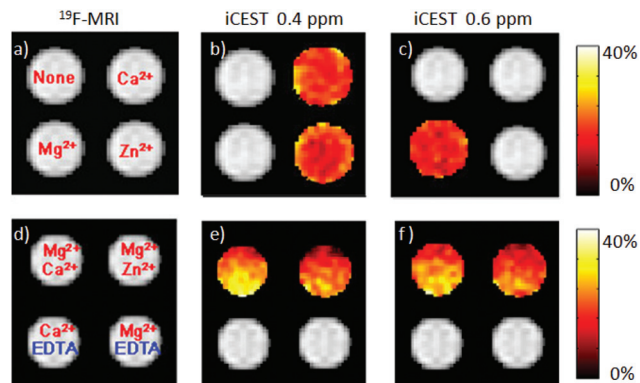


Fig. 5 ^{19}F iCEST MRI of chelator 4 in the presence of metal ions Mg^{2+} , Ca^{2+} , Zn^{2+} , and EDTA. Each sample contained 5 mM chelator 4 and 50 μM indicated metal ion, respectively. Samples d–f were added extra 50 μM of Mg^{2+} or 1 mM EDTA, respectively.

containing 5 mM chelator 4 and 50 μM of each metal ion showed no noticeable contrast (Fig. 5a). However, when a saturation pulse was applied at $\Delta\omega = 0.4$ ppm, ^{19}F iCEST images showed a clear contrast for the tubes containing Ca^{2+} and Zn^{2+} with a contrast percentile of 20% and 19%, respectively (Fig. 5b). When a saturation pulse was applied at $\Delta\omega = 0.6$ ppm, only the tube containing Mg^{2+} showed clear contrast ^{19}F iCEST images with a contrast percentile of 17% (Fig. 5c). Therefore, using chelator 4, it is feasible to selectively detect Mg^{2+} at $\Delta\omega = 0.6$ ppm and simultaneously detect both Ca^{2+} and Zn^{2+} at $\Delta\omega = 0.4$ ppm using ^{19}F iCEST MRI. Although the $\Delta\omega$ is pretty small, the chemical shift insensitive nature of free and metal ion bound-chelator 4 to pH, temperature, and fast exchange ions makes the ^{19}F iCEST MRI process straightforward. Secondly, the selective ^{19}F iCEST MRI of Mg^{2+} in the presence of Ca^{2+} , Zn^{2+} and *vice versa* was studied.

A clear contrast for Mg^{2+} at $\Delta\omega = 0.6$ ppm can still be observed in the presence of coexisting ions Ca^{2+} and Zn^{2+} (Fig. 5f). Meanwhile, it can also selectively detect Ca^{2+} and Zn^{2+} in the metal ion-bound chelator 4 compared to that of EDTA evaluated with ^{19}F iCEST MRI. In the presence of 1 mM EDTA, competing chelating reactions for metal ions between EDTA and chelator 4 took place. It turned out that Mg^{2+} , Ca^{2+} , and Zn^{2+} form a much more stable complex with EDTA than those of chelator 4 because no ^{19}F iCEST MRI was observed at either 0.4 ppm or 0.6 ppm. The association constant measurement of chelators 1–4 with Mg^{2+} , Ca^{2+} , and Zn^{2+} through a titration method¹¹ indicated that EDTA and DTPA have higher binding affinities towards these metal ions than those of the corresponding fluorinated chelators (Fig. S3 and Table S1 in the ESI†). Thus, the addition of EDTA can turn off the ^{19}F iCEST MRI by preventing the formation of metal ion bound-chelator 4. In this way, an on- and off- ^{19}F iCEST MRI strategy for selectively detecting metal ions can be developed. Because each metal ion has a quite unique stability constant with commercially available chelators, such as EDTA, DTPA, DOTA, *etc.*, it is possible to selectively turn off ^{19}F iCEST MRI by the

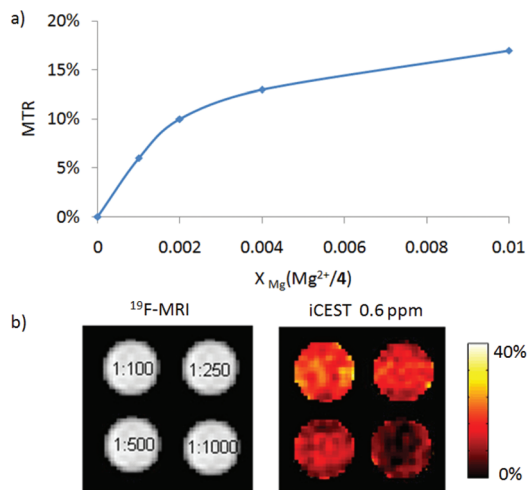


Fig. 6 (a) Plot of the magnetization transfer ratio (MTR) vs. X_{Mg} . (b) ^{19}F iCEST MRI of chelator 4 in the presence of Mg^{2+} . Alignment of four tubes containing 5 mM of 4 and different concentrations of Mg^{2+} ($X_{\text{Mg}} = 1:100$, 1:250, 1:500, 1:1000).

addition of a commercially available chelator to a metal ion mixture and selectively chelating the ^{19}F iCEST MRI-generating metal ion(s). Based on these observations, Mg^{2+} , Ca^{2+} , and Zn^{2+} can be sensitively and selectively detected with chelator 4 by ^{19}F iCEST MRI at a concentration as low as 50 μM .

To investigate the sensitivity of chelator 4 in detecting Mg^{2+} with ^{19}F iCEST MRI, a Mg^{2+} concentration-dependent ^{19}F iCEST MRI was then carried out (Fig. 6). It was found that Mg^{2+} can be detected at a concentration of 10 μM . In this case, a magnetization transfer ratio (MTR) of 11% was observed at a $\text{Mg}^{2+}/4$ ratio of 1:500 with a data collection time of 6.5 minutes.

Conclusions and prospects

In this study, we have developed a class of novel ^{19}F CEST imaging probes and applied them in sensitively and selectively detecting metal ions with ^{19}F iCEST MRI. These imaging probes with a strong and singlet ^{19}F NMR peak from multiple fluorines can be conveniently prepared on gram scales from commercially available chelators. Compared to the known fluorinated metal ion chelators, the ^{19}F NMR chemical shift of these chelators is not sensitive to the environment, *e.g.* pH and temperature, but it is sensitive to certain metal ions, which turns these chelators into selective ^{19}F imaging probes for these metal ions. However, the chemical shift change induced by the metal ions is quite low, <1 ppm, compared to 10.5 ppm from TF-BAPTA. By tuning the frequency of a saturation pulse, multiple ions, especially for Mg^{2+} , can be selectively detected by ^{19}F iCEST MRI with one of these probes. Because of the symmetrical distribution of twelve fluorines, the probe exhibits enhanced sensitivity for detecting metal ions at low concentrations. For imaging metal ions

in vivo with ^{19}F iCEST MRI, some fine tuning of sensitivity, selectivity, chelation properties, and physicochemical properties of the existing probes is always required. The study here has illustrated a fine tuning strategy to enhance the sensitivity of the ^{19}F imaging probe, while maintaining its metal ion selectivity by constructing novel fluorinated chelators. Further fine tuning of the structure of the probes to improve the selectivity to multiple metal ions is actively going on in this group.

Experimental

General information

The ^1H , ^{19}F and ^{13}C NMR spectra of chelators were recorded on a 400 MHz spectrometer. Chemical shifts are in ppm and coupling constants (J) are in hertz (Hz). ^1H NMR spectra were referenced to solvent hydrogens (3.31 ppm) using CD_3OD as a solvent. ^{13}C NMR spectra were referenced to solvent carbons (m, 49.64–48.36 ppm for CD_3OD). ^{19}F NMR spectra were referenced to 2% perfluorobenzene (s, -164.90 ppm) in CD_3OD or sodium trifluoromethanesulfonate (s, -79.61 ppm) in D_2O . The splitting patterns of the ^1H NMR spectra are denoted as follows: s (singlet), d (doublet), q (quartet), and m (multiplet). Unless otherwise indicated, all reagents were obtained from a commercial supplier and used without prior purification. DMF, Et_3N and pyridine were dried and freshly distilled prior to use.

^{19}F MRI experiments were performed on a 9.4 T micro-imaging system with a 10 mm inner diameter ^{19}F coil (376.4 MHz) for both radiofrequency transmission and reception. The RARE sequence was employed for all MRI acquisitions with single average. RARE factor = 4, TR = 6000 ms, TE = 5.37 ms, matrix = 32×32 , number of average = 4, FOV = $30 \text{ mm} \times 30 \text{ mm}$, slice thickness = 20 mm, saturation pulse strength = $1 \mu\text{T}$, saturation time = 3 s.

General procedure for the preparation of compounds 1–4 and compound 5. A slurry of EDTA (2.92 g, 10.00 mmol), dry pyridine (4.75 g, 60.00 mmol), and acetic anhydride (4.08 g, 40.00 mmol) was heated to 80°C and stirred at this temperature for 24 h. After cooling to room temperature, the reaction mixture was filtered. The solid residue was washed with acetic anhydride and diethyl ether to yield **5** as a white solid (2.56 g, yield 99%). ^1H NMR (400 MHz, d-DMSO): δ 3.70 (s, 8H), 2.66 (s, 4H).

Compound 6. Diethylenetriaminepentaacetic acid bis-anhydride **6** was prepared as a white solid (3.93 g, yield 99%) by following the same procedure as for **5**. ^1H NMR (400 MHz, d-DMSO): δ 2.60 (t, $J = 6.2$ Hz, 4H), 2.76 (t, $J = 6.2$ Hz, 4H), 3.44 (s, 2H), 3.72 (s, 8H).

Compound 7. To a sealed vessel were added 4-methylaniline (4.00 g, 37.33 mmol), 4-toluenesulfonic acid monohydrate (0.71 g, 3.73 mmol), 1,1,1,3,3,3-hexafluoroacetone trihydrate (12.32 g, 55.99 mmol) and toluene (25 mL). The vessel was sealed up and stirred for 8 h at 110°C . The solution was concentrated under vacuum and the residue was purified by flash chromatography on silica gel (petroleum ether/ethyl acetate = 9/1) to give compound **7** as white needles (6.93 g,

yield 68%). ^1H NMR (400 MHz, CDCl_3): δ 7.38 (s, 1H), 7.17 (d, $J = 8.0$ Hz, 1H), 6.97 (d, $J = 8.0$ Hz, 1H), 2.36 (s, 3H); ^{19}F NMR (376 MHz, CDCl_3): δ -78.41 .

Compound 1. To a stirring solution of EDTA dianhydride **5** (1.02 g, 4.00 mmol) in DMF (35 mL) and triethylamine (1.62 g, 16.00 mmol) was added a solution of amine **7** (0.55 g, 2.00 mmol) in 8 mL DMF dropwise under an atmosphere of nitrogen at 0°C . After the addition, the mixture was stirred at 0°C for 1 h and at room temperature for another 8 h. The reaction was quenched with H_2O and the solvent was evaporated under vacuum. The residue was purified with preparative RP-HPLC to give **1** (0.61 g, yield 56%) as a white solid. ^1H NMR (400 MHz, CD_3OD): δ 8.07 (d, $J = 8.2$ Hz, 1H), 7.38 (s, 1H), 7.32 (d, $J = 8.5$ Hz, 1H), 4.11 (s, 4H), 3.96 (s, 2H), 3.90 (s, 2H), 3.44 (t, $J = 5.4$ Hz, 2H), 3.35 (t, $J = 5.5$ Hz, 2H), 2.35 (s, 3H); ^{13}C NMR (100 MHz, CD_3OD): δ 172.3, 170.9, 168.7, 136.2, 135.9, 132.2, 129.4, 126.8, 124.4 (q, $J = 289.6$ Hz), 120.1, 82.0–80.9 (m), 58.5, 55.8, 53.5, 52.2, 21.0; ^{19}F NMR (376 MHz, CD_3OD): δ -74.69 ; HRMS (ESI) calcd for $\text{C}_{20}\text{H}_{22}\text{F}_6\text{N}_3\text{O}_8^-$ ($[\text{M} - \text{H}]^-$), 546.1317, found, 546.1328.

Compound 2. Chelator **2** was prepared as a white solid (1.30 g, yield 81%) by following the same procedure as for chelator **1**. ^1H NMR (400 MHz, CD_3OD): δ 8.08 (d, $J = 8.1$ Hz, 2H), 7.36 (s, 2H), 7.22 (d, $J = 8.1$ Hz, 2H), 3.84 (s, 4H), 3.80 (s, 4H), 3.25 (s, 4H), 2.33 (s, 6H). ^{13}C NMR (100 MHz, CD_3OD): δ 171.6, 167.7, 136.0, 132.1, 129.4, 126.9, 124.3 (q, $J = 288.4$ Hz), 121.2, 82.0–80.8(m), 58.4, 55.9, 53.1, 21.1; ^{19}F NMR (376 MHz, CD_3OD): δ -74.69 ; HRMS (ESI) calcd for $\text{C}_{30}\text{H}_{29}\text{F}_{12}\text{N}_4\text{O}_8^-$ ($[\text{M} - \text{H}]^-$), 801.1799, found, 801.1798.

Compound 3. To a stirring solution of DTPA dianhydride **6** (1.43 g, 4.00 mmol) and triethylamine (1.62 g, 16.00 mmol) in DMF (35 mL) was dropwise added amine **7** (0.55 g, 2.00 mmol) in DMF (8 mL) under an atmosphere of nitrogen at 0°C and the mixture was stirred at this temperature for 1 h. After warming to room temperature, the mixture was stirred at room temperature for additional 8 h. The reaction was quenched with H_2O and the solvent was evaporated under vacuum. The residue was purified with preparative RP-HPLC to give **3** (0.79 g, yield 61%) as a white solid. ^1H NMR (400 MHz, CD_3OD): δ 8.14 (d, $J = 8.6$ Hz, 1H), 7.38 (s, 1H), 7.33 (d, $J = 8.5$ Hz, 1H), 4.17 (s, 2H), 3.85 (s, 2H), 3.80 (s, 6H), 3.52–3.35 (m, 8H), 2.35 (s, 3H); ^{13}C NMR (100 MHz, CD_3OD): δ 174.4, 173.7, 170.8, 169.4, 136.6, 135.4, 132.2, 129.4, 125.9, 123.0, 120.2, 82.0–80.9 (m), 59.0, 56.0, 54.9, 54.7, 54.3, 51.3, 50.9, 21.0; ^{19}F NMR (376 MHz, CD_3OD): δ -74.64 ; HRMS (ESI) calcd for $\text{C}_{24}\text{H}_{29}\text{F}_6\text{N}_4\text{O}_{10}^-$ ($[\text{M} - \text{H}]^-$), 647.1793, found, 647.1796.

Compound 4. Chelator **4** was prepared as a white solid (2.25 g, yield 83%) by following the same procedure as for chelator **3**. ^1H NMR (400 MHz, CD_3OD): δ 8.09 (d, $J = 8.3$ Hz, 2H), 7.35 (s, 2H), 7.26 (d, $J = 8.5$ Hz, 2H), 4.19 (s, 2H), 3.78 (s, 4H), 3.73 (s, 4H), 3.48 (t, $J = 6.1$ Hz, 4H), 3.33 (t, $J = 6.2$ Hz, 4H), 2.33 (s, 6H); ^{13}C NMR (100 MHz, CD_3OD): δ 173.1, 169.9, 169.8, 136.3, 135.6, 132.2, 129.3, 126.3, 124.4 (q, $J = 288.7$ Hz), 120.6, 82.1–80.9 (m), 58.9, 56.0, 54.8, 54.1, 51.6, 21.0; ^{19}F NMR (376 MHz, CD_3OD): δ -74.69 ; HRMS (ESI) calcd for $\text{C}_{34}\text{H}_{36}\text{F}_{12}\text{N}_5\text{O}_{10}^-$ ($[\text{M} - \text{H}]^-$), 902.2276, found, 902.2259.

Acknowledgements

We are thankful for financial support from the National Key Research and Development Program of China (2016YFC1304704), the National Natural Science Foundation of China (21372181, 21402144 and 21572168), and the State Key Laboratory for Magnetic Resonance and Atomic and Molecular Physics (Wuhan Institute of Physics and Mathematics).

Notes and references

- (a) K. P. Carter, A. M. Young and A. E. Palmer, *Chem. Rev.*, 2014, **114**, 4564–4601; (b) R. Y. Tsien, *Biochemistry*, 1980, **19**, 2396–2404; (c) G. A. Smith, R. T. Hesketh, J. C. Metcalfe, J. Feeney and P. G. Morris, *Proc. Natl. Acad. Sci. U. S. A.*, 1983, **80**, 7178–7182; (d) F. A. X. Schanne, T. L. Dowd, R. K. Gupta and J. F. Rosen, *Proc. Natl. Acad. Sci. U. S. A.*, 1989, **86**, 5133–5135; (e) H. Komatsu, T. Miki, D. Citterio, T. Kuboba, Y. Shindo, Y. Kitamura, K. Oka and K. Suzuki, *J. Am. Chem. Soc.*, 2005, **127**, 10798–10799; (f) T. Nishihara, Y. Kameyama, H. Nonaka, Y. Takakusagi, F. Hyodo, K. Ichikawa and S. Sando, *Chem. – Asian J.*, 2017, **12**, 949–953.
- (a) E. T. Ahrens, R. Flores, H. Xu and P. A. Morel, *Nat. Biotechnol.*, 2005, **23**, 983–987; (b) J. M. Janjic, M. Srinivas, D. K. Kadayakkara and E. T. Ahrens, *J. Am. Chem. Soc.*, 2008, **130**, 2832–2841; (c) Z.-X. Jiang, X. Liu, E. K. Jeong and Y. B. Yu, *Angew. Chem., Int. Ed.*, 2009, **48**, 4755–4758; (d) J. Ruiz-Cabell, B. P. Barnett, P. A. Bottomley and J. W. M. Bulte, *NMR Biomed.*, 2011, **24**, 114–129; (e) D. Vivian, K. Cheng, S. Khuranan, S. Xu, E. H. Kriel, P. A. Dawson, J. P. Raufman and J. E. Polli, *Mol. Pharm.*, 2014, **11**, 1575–1582; (f) S. Langereis, J. Keupp, J. L. J. van Velthoven, I. H. C. de Roos, D. Burdinski, J. A. Pikkemaat and H. Gröll, *J. Am. Chem. Soc.*, 2009, **131**, 1380–1381.
- (a) C. Zhang, S. S. Moonshi, H. Peng, S. Puttick, J. Reid, S. Bernardi, D. J. Searles and A. K. Whittaker, *ACS Sens.*, 2016, **1**, 757–765; (b) D. Xie, S. Kim, V. Kohli, A. Banerjee, M. Yu, J. S. Enriquez, J. J. Luci and E. L. Que, *Inorg. Chem.*, 2017, **56**, 6429–6437; (c) T. Nakamura, H. Matsushita, F. Sugihara, Y. Yoshioka, S. Mizukami and K. Kikuchi, *Angew. Chem., Int. Ed.*, 2015, **54**, 1007–1010.
- (a) R. Hagen, J. P. Warren, D. H. Hunter and J. D. Roberts, *J. Am. Chem. Soc.*, 1973, **95**, 5712–5716; (b) N. Illy, D. Majonis, I. Herrera, O. Ornatsky and M. A. Winnik, *Biomacromolecules*, 2012, **13**, 2359–2369; (c) J. S. Summers, J. B. Baker, D. Meyerstein, A. Mizrahi, I. Zilbermann, H. Cohen, C. M. Wilson and J. R. Jones, *J. Am. Chem. Soc.*, 2008, **130**, 1727–1734.
- (a) G. E. Fryxell, W. Chouyok and R. D. Rutledge, *Inorg. Chem. Commun.*, 2011, **14**, 971–974; (b) J. C. Joyner, L. Hocharoen and J. A. Cowan, *J. Am. Chem. Soc.*, 2012, **134**, 3396–3410; (c) L. Tahsini, S. E. Specht, J. S. Lum, J. J. M. Nelson, A. F. Long, J. A. Golen, A. L. Rheingold and L. H. Doerrer, *Inorg. Chem.*, 2013, **52**, 14050–14063; (d) S. A. Cantalupo, S. R. Fiedler, M. P. Shores, A. L. Rheingold and L. H. Doerrer, *Angew. Chem., Int. Ed.*, 2012, **51**, 1000–1005.
- (a) A. Bar-Shir, A. A. Gilad, K. W. Y. Chan, G. Liu, P. C. M. van Zijl, J. W. M. Bulte and M. T. McMahon, *J. Am. Chem. Soc.*, 2013, **135**, 12164–12167; (b) A. Bar-Shir, N. N. Yadav, A. A. Gilad, P. C. M. van Zijl, M. T. McMahon and J. W. M. Bulte, *J. Am. Chem. Soc.*, 2015, **137**, 78–81.
- S. S. Kelkar, L. Xue, S. R. Turner and T. M. Reineke, *Biomacromolecules*, 2014, **15**, 1612–1624.
- (a) W. Yu, Y. Yang, S. Bo, Y. Li, S. Chen, Z. Yang, X. Zheng, Z.-X. Jiang and X. Zhou, *J. Org. Chem.*, 2015, **80**, 4443–4449; (b) S. Bo, C. Song, Y. Li, W. Yu, S. Chen, X. Zhou, Z. Yang, X. Zheng and Z.-X. Jiang, *J. Org. Chem.*, 2015, **80**, 6360–6366; (c) Y. Li, G. Xia, Q. Guo, L. Wu, S. Chen, Z. Yang, W. Wang, Z.-Y. Zhang, X. Zhou and Z.-X. Jiang, *MedChemComm*, 2016, **7**, 1672–1680.
- (a) M. Peana, S. Medici, V. M. Nurchi, J. I. Lachowicz, G. Crisponi, M. Crespo-Alonso, M. A. Santos and M. A. Zoroddu, *J. Inorg. Biochem.*, 2014, **141**, 132–143; (b) D. A. Dickie and R. A. Kemp, *Organometallics*, 2014, **33**, 6511–6518.
- R. F. Evilia, *Inorg. Chem.*, 1985, **24**, 2076–2080.
- (a) J. Bjerrum, *Metal Ammine Formation in Aqueous Solution*, P. Haase and Son, Copenhagen, 1941; (b) M. Calvin and K. W. Wilson, *J. Am. Chem. Soc.*, 1945, **67**, 2003–2007; (c) S. Chaberek Jr. and A. E. Martell, *J. Am. Chem. Soc.*, 1952, **74**, 5052–5056; (d) N. Türkel, *J. Chem. Eng. Data*, 2011, **56**, 2337–2342.